ADVANCED MATERIALS
www.advmat.de



# Efficient and Layer-Dependent Exciton Pumping across Atomically Thin Organic–Inorganic Type-I Heterostructures

*Linglong Zhang, Ankur Sharma, Yi Zhu, Yuhan Zhang, Bowen Wang, Miheng Dong, Hieu T. Nguyen, Zhu Wang, Bo Wen, Yujie Cao, Boqing Liu, Xueqian Sun, Jiong Yang, Ziyuan Li, Arara Kar, Yi Shi, Daniel Macdonald, Zongfu Yu, Xinran Wang,* and Yuerui Lu**

**The fundamental light–matter interactions in monolayer transition metal dichalcogenides might be significantly engineered by hybridization with their organic counterparts, enabling intriguing optoelectronic applications. Here, atomically thin organic–inorganic (O–I) heterostructures, comprising monolayer $MoSe_2$ and mono-/few-layer single-crystal pentacene samples, are fabricated. These heterostructures show type-I band alignments, allowing efficient and layer-dependent exciton pumping across the O–I interfaces. The interfacial exciton pumping has much higher efficiency (>86 times) than the photoexcitation process in $MoSe_2$, although the pentacene layer has much lower optical absorption than $MoSe_2$. This highly enhanced pumping efficiency is attributed to the high quantum yield in pentacene and the ultrafast energy transfer between the O–I interface. Furthermore, those organic counterparts significantly modulate the bindings of charged excitons in monolayer $MoSe_2$ via their precise dielectric environment engineering. The results open new avenues for exploring fundamental phenomena and novel optoelectronic applications using atomically thin O–I heterostructures.**

Van der Waals (vdW) heterostructures (HS) have in-plane covalently bonded atomic layers which facilitate the formation of well-defined interfaces with absence of any dangling bonds.[1] The constituent layers interact weakly with out-of-plane layers and this weak vdW interaction enables the stacking of atomically thin layers on each other with precision. Semiconducting transition metal dichalcogenides (TMDCs) are important building blocks for fabricating 2D vdW heterostructures that possess atomically sharp interfaces, enabling promising optoelectronic applications such as efficient photodetectors, light-emitting diodes, resonant tunneling diodes, and solar cells.[2–4] Organic molecular semiconductors have also recently been integrated with 2D TMDCs to form vdW heterostructures,[5–10] which can dramatically engineer the light–matter interactions in the hybrid system and allow for new types of optoelectronic devices. However, those organic counterparts reported were based on bulk organic materials (>20 nm thick). The organic molecular arrangements on those reported O–I interfaces were not well controlled on the atomic scale, although the optoelectronic properties of organic molecular crystals are typically very sensitive to its aggregation and molecular arrangements.[11–13] Compared to their bulk counterparts, our recently reported atomically thin high-quality 2D organic molecular crystals possess well-defined molecular arrangements and the interesting layer-dependent carrier transport properties.[14,15] This will allow us to build atomically thin O–I interfaces with well-controlled molecular arrangements on the interface and explore how the molecular aggregations would affect the light–matter interactions in the hybrid system. Furthermore,

Dr. L. Zhang, Dr. Y. Zhang, Dr. Y. Cao, Prof. Y. Shi, Prof. X. Wang
National Laboratory of Solid State Microstructures
Collaborative Innovation Center of Advanced Microstructures
School of Electronic Science and Engineering
Nanjing University
Nanjing 210093, P. R. China
E-mail: xrwang@nju.edu.cn

Dr. L. Zhang, Dr. A. Sharma, Dr. Y. Zhu, Dr. B. Wang, Dr. M. Dong, Dr. H. T. Nguyen, Dr. B. Wen, Dr. B. Liu, Dr. X. Sun, Dr. J. Yang, Dr. A. Kar, Prof. D. Macdonald, Prof. Y. Lu
Research School of Engineering
College of Engineering and Computer Science
The Australian National University
Canberra, Australian Capital Territory 2601, Australia
E-mail: yuerui.lu@anu.edu.au

Dr. Z. Wang, Dr. Z. Yu
Department of Electrical and Computer Engineering
University of Wisconsin
Madison, WI 53706, USA

Dr. Z. Li
Department of Electronic Materials Engineering
Research School of Physics and Engineering
The Australian National University
Canberra 2601, ACT, Australia

Prof. Y. Lu
ARC Centre of Excellence in Future Low-Energy Electronics Technologies (FLEET)
ANU node
Canberra, Australian Capital Territory 2601, Australia

DOI: 10.1002/adma.201803986

 

ultrathin organic molecular crystals have a clear interface and high excitonic densities with high binding energies,[16] which can comprehensively interact with excitonic states in the inorganic 2D materials and can lead to various applications for optical devices such as light-emitting devices.[17–19]

Here, we demonstrated atomically thin O–I heterostructures, by stacking exfoliated monolayer $MoSe_2$ onto mono-/few-layer single-crystal pentacene samples that were epitaxially grown over h-BN surfaces. We observed significant photoluminescence (PL) enhancement from the monolayer $MoSe_2$ and PL quenching in the pentacene layers. Photoluminescence exciton (PLE) measurements were used to prove the type-I band alignments. The atomically thin O–I heterostructures with well-controlled interfacial molecular arrangements and type-I band alignments allow us to study the efficient and layer-dependent exciton pumping across the high-quality O–I interfaces which is in contrast to previously reported O–I heterostructures[5,6,14,20,21] (with type-II band alignments). The interfacial exciton pumping efficiency from the hybridization of a wetting layer pentacene (0.5 nm thick) was measured to be ≈86 times higher than that from the photoexcitation process in $MoSe_2$, although the pentacene layer has much lower optical absorption than $MoSe_2$. The highly enhanced pumping efficiency is attributed to the high quantum yield (QY) in pentacene and the ultrafast energy transfer between the O–I interface. The measured interfacial pumping efficiency was sensitive to the layer number of organic 2D materials. Moreover, compared with other substrates, such as $SiO_2$ and h-BN, the pentacene layer has highly reduced dielectric screening effect on the many-body interactions in $MoSe_2$, which resulted in the enhanced bindings of the charged excitons in monolayer $MoSe_2$ depending on the spacing thickness of pentacene layer.[22] Our findings provide a new way to engineer the light–matter interactions in atomically thin semiconductors and their hybrids, enabling various new optoelectronic devices, such as ultrathin lighting diodes, heterostructure lasers, etc.

**Figure 1**a shows the schematic configuration of the heterostructure. First, few layers of h-BN were mechanically exfoliated onto a 290 nm $Si/SiO_2$ substrate. Then the ultrathin 2D pentacene films were subsequently grown on the exfoliated h-BN via the physical vapor deposition (PVD) method in a tube furnace. The growth process is detailed in the author's previous work.[14] $MoSe_2$ monolayer was then exfoliated and stacked on the atomically thin pentacene layers to form the heterostructures.[23] This technique is a better method to avoid contamination and damage of the organic materials during the transfer process, and achieves ultraclean and intact atomic interfaces.[24] Figure 1b,c shows the optical microscopy images of before and after transfer of monolayer $MoSe_2$ onto the pentacene film, respectively. The interfacial layer of pentacene grown directly over the h-BN is referred to as the wetting layer (WL) and subsequent layers above the WL are referred to as 1L and 2L.[14] After heterostructure, all individual heterostructures are characterized by Raman spectroscopy after stacking (see Figure S1, Supporting Information) to confirm the formation of heterostructure. Atomic force microscopy (AFM) (Figure 1d and Figure S2, Supporting Information) was further used to deterministically designate each pentacene layer based on the observed thickness. Three different heterostructures based on the thickness of pentacene layers underneath the monolayer $MoSe_2$ were fabricated. The optical image after stacking shown in Figure 1c shows three distinct heterostructure regions. PL spectroscopy is a sensitive probe to study the dynamic interlayer and intralayer charge transfer excitonic states which can provide evidence of coupling between the individual heterostructure layers.[2,24,25] The PL spectra of the various heterostructures are shown in Figure 1e, an excitonic peak around 788 nm was observed for $MoSe_2$ (olive curve) and pentacene showed a broad emission in the range of 550–700 nm (red curve). The PL peak intensity of the 1L $MoSe_2$ + WL PEN heterostructure at ≈788 nm clearly indicates ≈2.8 times enhancement (Figure 1e I) as compared to that of monolayer $MoSe_2$ on $SiO_2/Si$ substrate, whereas the PL peak from pentacene has been quenched. The enhancement factor $\eta$ is defined as the ratio of absolute PL intensities of a HS to that of the monolayer $MoSe_2$ on $SiO_2/Si$ substrate at 788 nm as observed during the experiments (i.e., $\eta = I_{HS}/I_{MoSe_2}$). Slightly lower enhancements were observed in the 1L $MoSe_2$ + 1L PEN($\eta \approx 2.4$, Figure 1e II), 1L $MoSe_2$ + 2L PEN ($\eta \approx 1.7$, Figure 1e III), and 1L $MoSe_2$ + bulk PEN ($\eta \approx 1.2$, Figure S3, Supporting Information) heterostructures. Several devices (>5) were tested and these results were repeatable after numerous measurements. Also, we tested the heterostructures of 1L $MoSe_2$ on 2D pentacene after one month and the enhancement factor was observed to be stable, as compared with the initial measurements (Figure S4, Supporting Information).

In heterostructure design, the relative band alignment is the key factor that determines the type of heterostructure.[26] **Figure 2**a illustrates the alignment of electronic bands of pentacene and $MoSe_2$,[27–29] where the $MoSe_2$/pentacene forms a type-I heterojunction. Specifically, the highest occupied molecular orbital (HOMO) of pentacene is lower than the valence band maximum (VB) of monolayer $MoSe_2$ and the lowest unoccupied molecular orbital (LUMO) of pentacene is higher than the conduction band minimum (CB) of monolayer $MoSe_2$. As shown in Figure 2a, photoexcited carriers would transfer from pentacene to $MoSe_2$ due to large inbuilt potential and combine radiatively, which leads to the enhancement of the PL intensity in the $MoSe_2$ layer and the quenching of the PL intensity in pentacene layer (Figure 1e).

To further confirm the type-I band alignment nature of O–I hybrid heterostructures, photoluminescence excitation (PLE) experiments at room temperature were conducted. As shown in Figure 1e, the exciton peak position of 1L $MoSe_2$ is ≈788 nm (1.57 eV), which matches well with previous results.[30–32] Pentacene has a broad exciton peak shape at 585 nm (2.12 eV).[6,14] It implies that pentacene's lowest excited energy should be larger than that of monolayer $MoSe_2$. Figure 2b,c shows the PL spectra from 1L $MoSe_2$ and the 1L $MoSe_2$ + WL PEN heterostructure with excitation wavelength of 532 nm (2.33 eV) and 750 nm (1.65 eV), respectively. Figure 2b shows the PL intensity enhancement factor ($\eta$) is still around 2.8 which matches well with PL spectrum of Figure 1e. This is due to both the $MoSe_2$ and pentacene layers of the heterojunction were excited with an excitation energy of 2.33 eV. The photoexcited carriers can only transfer from the pentacene layer to $MoSe_2$ if the band alignment is type-I. Specifically, both electrons and holes are expected to transfer to $MoSe_2$ (see Figure 2a). In contrast, under an excitation wavelength of 750 nm as shown in Figure 2c, the PL intensity from 1L $MoSe_2$ + WL PEN

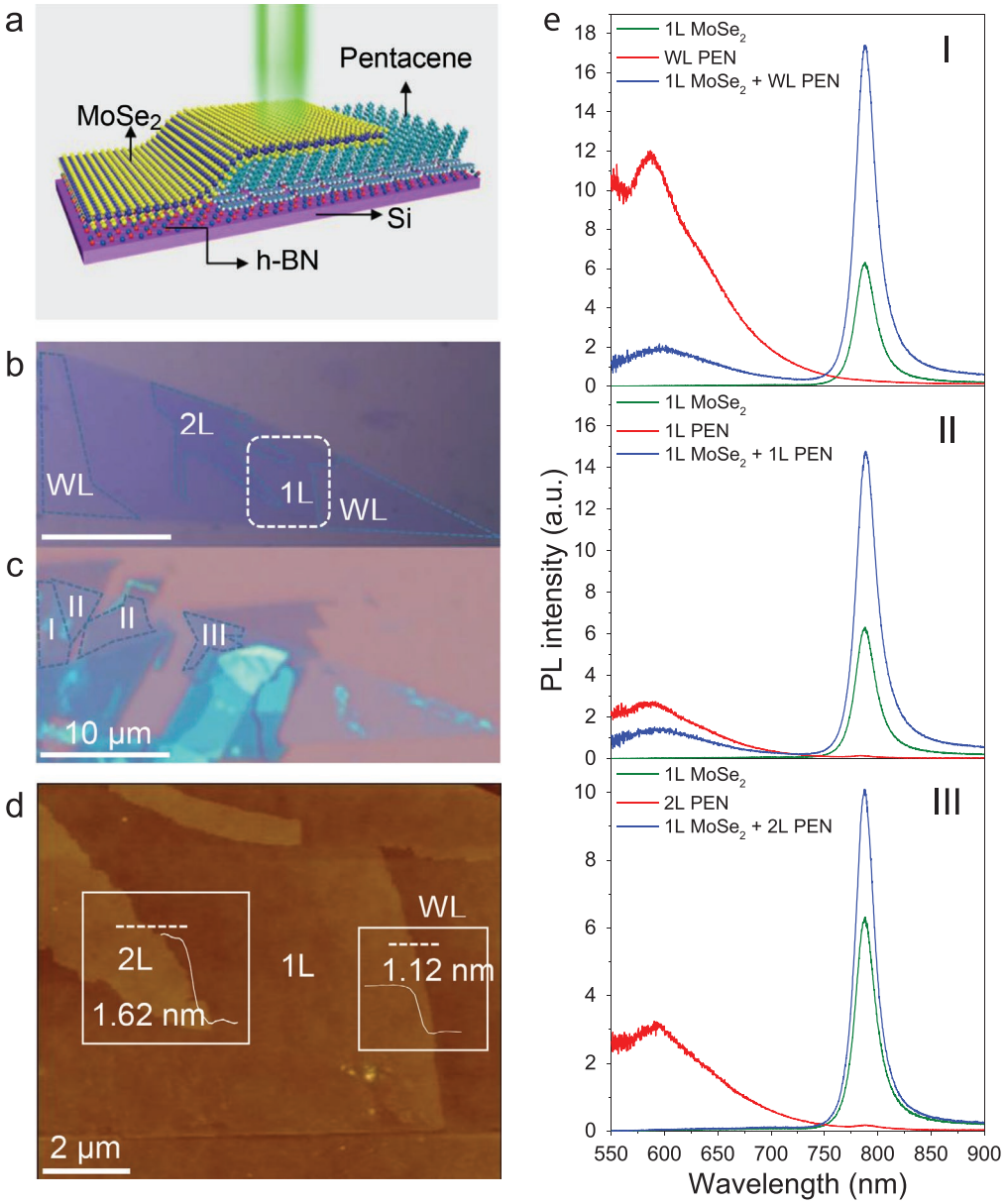


**Figure 1.** Characterization of layer-dependent heterostructures comprising of monolayer $MoSe_2$ and 2D pentacene. a) Schematic diagram of heterostructure of monolayer $MoSe_2$ on 2D pentacene. b) Optical image before heterostructure formation showing wetting layer (WL), one-layer (1L), and two-layer (2L) pentacene regions. Scale bar: 10 μm. c) Optical image after 1L $MoSe_2$ transferred on pentacene. Scale bar: 10 μm. (I) Heterostructure of 1L $MoSe_2$ on WL pentacene (1L $MoSe_2$ + WL PEN). (II) Heterostructure of 1L $MoSe_2$ on 1L pentacene (1L $MoSe_2$ + 1L PEN). (III) Heterostructure of 1L $MoSe_2$ on 2L pentacene (1L $MoSe_2$ + 2L PEN). Scale bar: 10 μm. d) AFM image of the dotted rectangular area shown in (b). Inset: height measurements along the dashed line showing atomic layer thickness. e) (I) PL spectra of 1L $MoSe_2$ + WL PEN heterostructure, 1L $MoSe_2$, and WL PEN. (II) PL spectra from 1L $MoSe_2$ + 1L PEN heterostructure, 1L $MoSe_2$, and 1L PEN. (III) PL spectra from 1L $MoSe_2$ + 2L PEN heterostructure, 1L $MoSe_2$, and 2L PEN.

heterostructure is comparable to that of monolayer $MoSe_2$ on $SiO_2$/Si substrate. In this case with 750 nm excitation, only the $MoSe_2$ layer was excited since the lowest excitonic energy of pentacene is ≈1.83 eV (Figure 1e).[33] The PL intensity from the heterostructure was slightly higher (≈1.19 times) than that from the 1L $MoSe_2$ sample on $SiO_2$/Si substrate (Figure 2c). This small PL enhancement might be due to that the pentacene layer acts as a passive layer decreasing nonradiative decay from the substrate or interface, which can be supported by the slightly increased carrier lifetime for exciton (≈788 nm) peak of heterostructure than that of 1L $MoSe_2$ sample on $SiO_2$/Si (Figure S5, Supporting Information).[34,35] From the PLE measurement (Figure 2d), PL intensity ratio (i.e., $\eta$) decreases sharply over excitation wavelengths of 700–750 nm, which corresponds to the lowest excitonic energy band in pentacene.[33] The PLE data clearly confirm the type-I band alignment in our 1L $MoSe_2$ + WL PEN heterostructure. Similar PLE measurements were conducted to confirm the type-I band alignments in 1L $MoSe_2$ + 1L PEN and 1L $MoSe_2$ + 2L PEN heterostructures as shown in Figure S6 (Supporting Information).

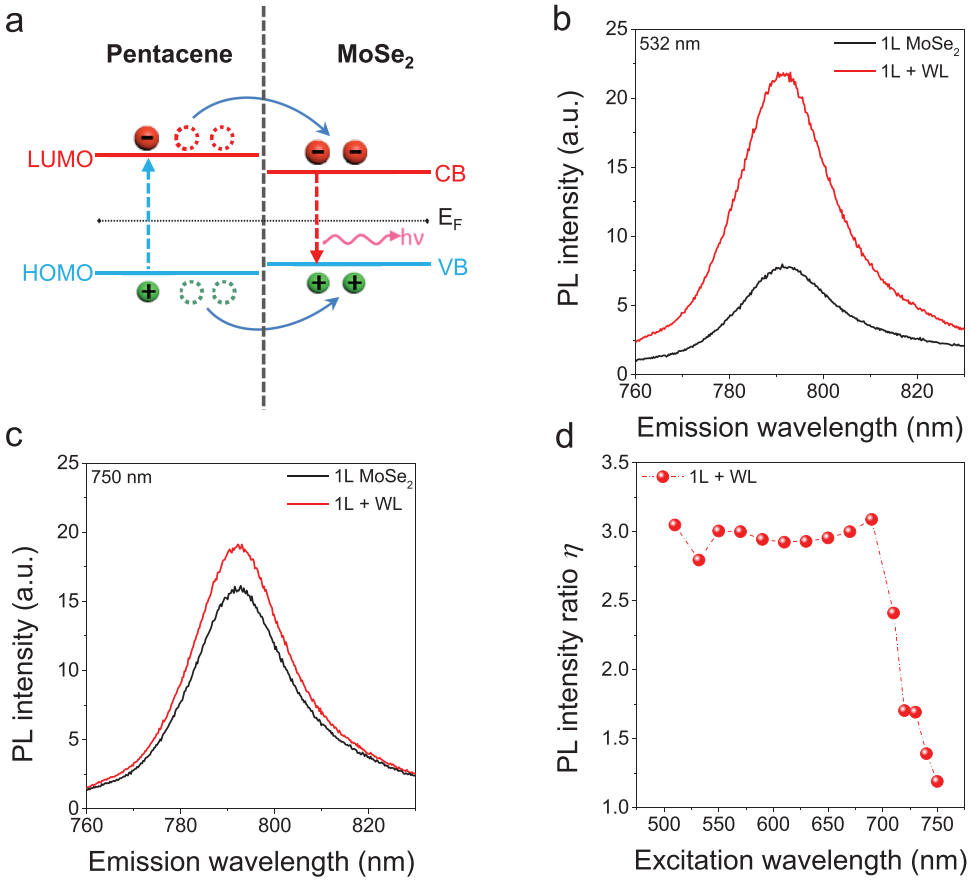


**Figure 2.** Confirmation of type-I band alignment by photoluminescence excitation (PLE). a) Band alignment diagram of a $MoSe_2$/pentacene heterostructure, which forms a type I heterostructure. b,c) Measured PL spectra of 1L $MoSe_2$ from $SiO_2$/Si substrate and from 1L $MoSe_2$ + WL PEN heterostructure, with different excitation wavelengths: 532 and 750 nm. d) Measured PL enhancement factor $\eta$ from 1L $MoSe_2$ + WL PEN heterostructure as a function of excitation wavelength. The enhancement factor $\eta$ is defined as the intensity ratio of PL peak at ≈788 nm between a heterostructure (HS) and the monolayer $MoSe_2$ on $SiO_2$/Si substrate.

The type-I band alignments in our atomically thin O–I heterostructures allow the efficient exciton pumping across the O–I interfaces. The hybridization of a WL pentacene (≈0.5 nm) leads to PL enhancement of 2.8 times. Considering that the WL pentacene has much lower measured optical absorption than 1L $MoSe_2$ (≈51 times lower) at the excitation wavelength of 532 nm (see Table S1, Supporting Information, and associated text), the exciton pumping efficiency across the O–I interface should be much higher than that from photoexcitation process in 1L $MoSe_2$. To further analyze the pumping efficiencies in the different heterostructures, an internal exciton pumping efficiency enhancement factor ($\beta$) is defined as

$$\beta = \frac{\text{Exciton pumping efficiency from heterostructure}}{\text{Exciton pumping efficiency from photoexciton in TMD}} = \left(\frac{I_{HS} - I_{TMD}}{I_{TMD}}\right)\left(\frac{A_{TMD}}{A_{PEN}}\right) \quad (1)$$

where $I_{HS}$ and $I_{TMD}$ are the measured integrated PL intensity from the HS and 1L $MoSe_2$ on $SiO_2$/Si substrate, respectively. $A_{TMD}$ and $A_{PEN}$ represent the measured absorption value from monolayer $MoSe_2$ and pentacene, respectively (Note S3 and Table S1, Supporting Information). The measured $\beta$ values for the 1L $MoSe_2$ + WL, 1L $MoSe_2$ + 1L PEN, and 1L $MoSe_2$ + 2L PEN heterostructures were 86.4, 20.4, and 3.2, respectively, which decrease with increasing thickness of pentacene film (**Figure 3**a), similar trend with the thickness-normalized PL intensities. The $\beta$ values are highly related to the QYs (Note S4, Supporting Information) and carrier lifetimes in both layers,[36] photocarrier relaxation pathways, and energy transfer channels (Figure 3b). In the 1L $MoSe_2$ + WL PEN heterostructure under 532 nm laser excitation, both the $MoSe_2$ and pentacene would be excited. The charge transfer process between O–I interfaces is typically ultrafast (6.7 ps, for instance),[6,37,38] which is much shorter than the measured carrier lifetime in pentacene (1128 ps) and that in monolayer $MoSe_2$ (448 ps) (Figure 3c).[35] Therefore, a large fraction of pentacene photoexcited charges (both electrons and holes) could transfer quickly to the $MoSe_2$ side and relax to some excited states for radiative recombination. Also, because WL pentacene has much higher QY and much lower optical absorption (Note S3 and S4 and Table S1, Supporting Information) than 1L $MoSe_2$, the interfacial exciton pumping efficiency in our atomically thin heterostructures will be much higher than that from the photoexcitation process in 1L $MoSe_2$, thus a high $\beta$ value.

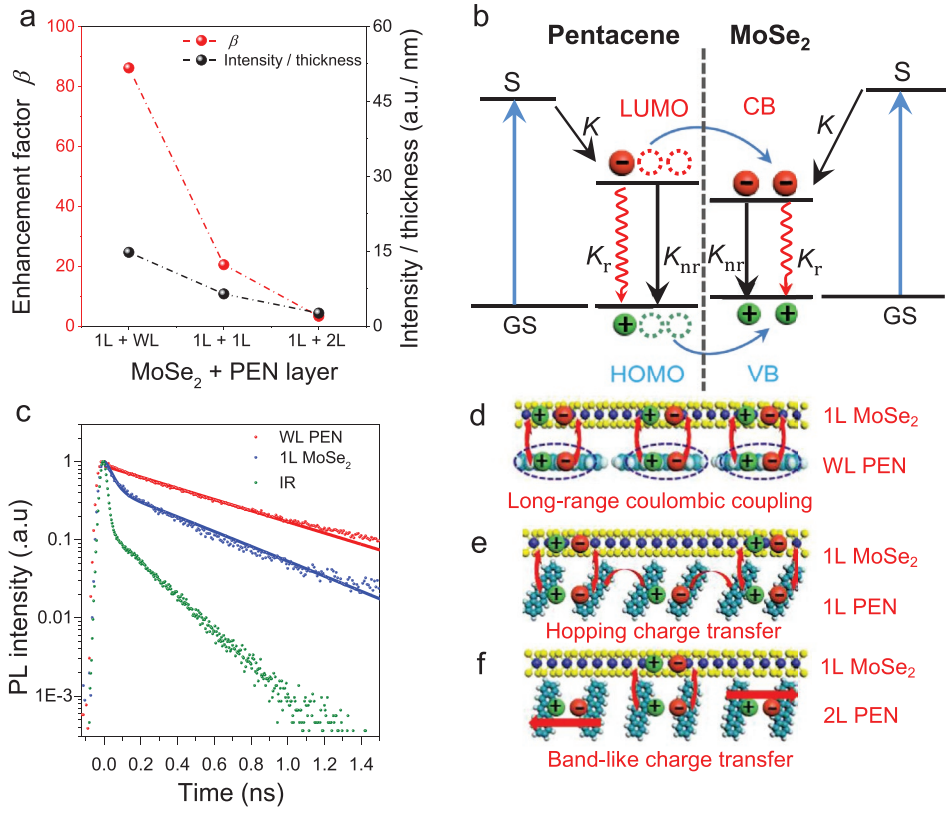


**Figure 3.** Efficient and layer-dependent interfacial exciton pumping. a) Exciton pumping efficiency enhancement factor $\beta$ (left), normalized PL intensity (by pentacene layer thickness) of various kinds of heterostructures as compared with 1L $MoSe_2$ (right). b) Schematic of the exciton relaxation channels in the $MoSe_2$/pentacene heterostructure for excitation at S state resonance. GS represents ground state and S represents the excitation state. The wavy red ($K_r$) and straight black arrows ($K_{nr}$) represent radiative and nonradiative decay process, respectively. $K$ is associated with each transition including intravalley thermalization or intervalley scattering. c) Measured time-resolved PL traces at room temperature for exciton peak ≈788 nm from oxide-supported monolayer $MoSe_2$ and for peak ≈590 nm from WL pentacene samples, IR represents instruments response curve. Based on the deconvolution with respect to the instrument response, double exponential equation $I = A\exp(-\frac{t}{\tau_1}) + B\exp(-\frac{t}{\tau_2}) + C$ was used for the fitting. For 1L $MoSe_2$, $\tau_1$ and $\tau_2$ were extracted to be 36 and 448 ps, respectively, which are considered to be nonradiative and radiative lifetimes, respectively.[30,34,35] For WL pentacene, the single exponential equation $I = A\exp(-\frac{t}{\tau}) + C$, $\tau$ was extracted to be 1128 ps. d) Schematic diagram shows the charge transfer between WL PEN (bottom) and 1L $MoSe_2$ (top). The dotted ellipse shows long-range intralayer coulombic coupling within WL PEN. e) Schematic diagram shows the charge transfer 1L PEN (bottom) and 1L $MoSe_2$ (top). The horizontal crooked arrows show the hopping mechanism of charge transfer within 1L PEN. f) Schematic diagram shows the charge transfer between 2L PEN (bottom) and 1L $MoSe_2$ (top). The horizontal arrows show the band-like mechanism of charge transfer within 2L PEN.

The layer-dependent $\beta$ values are highly related to the layer-dependent charge transport properties in 2D pentacene.[14] As described in our previous report,[14] WL pentacene was not conductive owing to the absence of intralayer $\pi$–$\pi$ stacking. The photoexcited electrons and holes in the WL are coupled through long-range coulombic forces (Figure 3d) and are immobile within the layer.[14] These localized charges can move more efficiently across the interface of the heterostructure into the $MoSe_2$. In 1L pentacene, charges are slightly more mobile within the pentacene layer and move through a hopping mechanism and are slightly more diffused along the pentacene layer (Figure 3e).[14] Some charges diffuse and rest then transfer across the interface into the $MoSe_2$ layer, this results in fewer exciton pairs recombining and a lower enhancement of PL intensity from the 1L $MoSe_2$ + 1L PEN heterostructure. Moreover, the lower relative QYs of 1L pentacene as compared to WL pentacene (Note S4, Supporting Information) also contribute to the smaller $\beta$ value. In 2L pentacene, the charges are extremely mobile and almost follow a band-like mechanism to move within the pentacene layer (Figure 3f).[14] Hence, the charges will be more diffused along the pentacene layer rather than crossing over the interface of the junction into the $MoSe_2$ layer. Furthermore, 2L pentacene has the lowest relative QYs among these pentacene films (Note S4, Supporting Information), in this case, fewer photocarriers transfer to the $MoSe_2$ and subsequently leads to the small $\beta$ value and low normalized PL intensity as shown in Figure 3a. In addition, bulk pentacene thin film has the lowest (almost ignorable) PL enhancement factor ($\eta \approx 1.2$, Figure S3, Supporting Information) and thus ultralow interlayer charge transfer efficiency, because bulk pentacene layer possesses the band-like charge transport mechanism (similar to 2L pentacene layer) but more traps and disorders in the thin film.[14] The comparison clearly shows that the efficient exciton pumping is only prominent at the 2D limit.

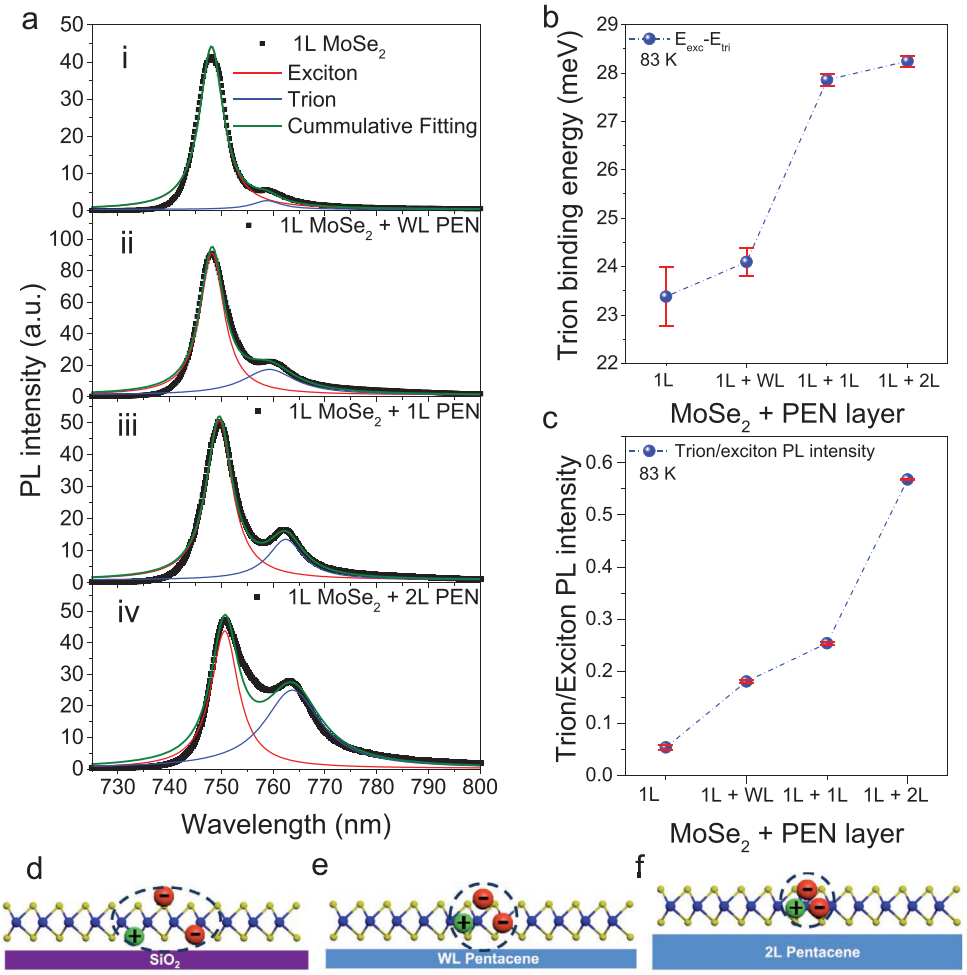


**Figure 4.** Layer-dependent modulation of the trion binding energy in 1L $MoSe_2$ via dielectric engineering. a) Measured PL spectra of 1L $MoSe_2$ from $SiO_2$/Si substrate, 1L $MoSe_2$ + WL PEN, 1L $MoSe_2$ + 1L PEN, and 1L $MoSe_2$ + 2L PEN heterostructures at 83 K. The PL spectrum was fitted by Lorenz function (black scatter lines are experimental data, red lines are labeled as exciton Peak, blue lines are labeled as trion peak, and olive lines are the cumulative fitting results). b) Measured trion binding energy (energy difference between exciton and trion peaks) of 1L $MoSe_2$ from $SiO_2$/Si substrate, 1L $MoSe_2$ + WL PEN, 1L $MoSe_2$ + 1L PEN, and 1L $MoSe_2$ + 2L PEN heterostructures at 83 K. c) Measured trion/exciton PL peak intensity ratio of 1L $MoSe_2$ from $SiO_2$/Si substrate, 1L $MoSe_2$ + WL PEN, 1L $MoSe_2$ + 1L PEN, and 1L $MoSe_2$ + 2L PEN heterostructures at 83 K. d–f) Schematic representation of negatively charged trions in 1L $MoSe_2$ over different substrates: $SiO_2$, WL PEN, and 2L PEN. Pentacene has lower dielectric constant than $SiO_2$ and h-BN. The PEN layer serves as a low-dielectric spacing layer, which provides reduced dielectric screening and leads to enhanced trion binding energy (smaller trion size) in 1L $MoSe_2$.

The strong many-body interactions in monolayer TMDs lead to the formation of robust quasi-particles, such as excitons, trions (charged excitons), and biexciton which are extremely important for the optoelectronics device applications, such as light-emitting diodes, optical modulators, etc.[30,39] Besides the efficient interfacial exciton pumping, the hybridization of 2D organic layers in our ultrathin O–I heterostructures would also allow us to precisely modulate the many-body interactions in the monolayer TMD via engineering the dielectric environment (**Figure 4**).[32,40] Temperature-dependent (Figure S7, Supporting Information) and gate-dependent PL measurements (Figure S8, Supporting Information) were conducted to explore the detailed modulation of many-body interactions in our heterostructure systems. In the PL spectra measured from the 1L $MoSe_2$ sample on $SiO_2$/Si substrate and in three heterostructures at 83 K, the two PL peaks at ≈748 and ≈759 nm (Figure 4a) are assigned to be the excitons and trions peaks of 1L $MoSe_2$, respectively.[30] Based on the gate-dependent measurements (Figure S8, Note S5, Supporting Information), those trion peaks as shown in Figure 4a are negatively charged. The binding energy of trion in 1L $MoSe_2$, energy difference between exciton and trion peak position,[32,41] was clearly enhanced with the hybridization of organic 2D materials and this enhancement increases with increasing pentacene layer number (Figure 4b). For instance, 1L $MoSe_2$ on $SiO_2$/Si sample showed a measured trion binding energy of ≈23.4 meV, which matches well with the reported value.[32,42] The trion binding energy of 1L $MoSe_2$ on 2L PEN is enhanced by 4.9 meV as compared with that of 1L $MoSe_2$ on $SiO_2$/Si (Figure 4b). The

PL intensity ratio between trion and exciton peaks was also enhanced with the hybridization of pentacene and this enhancement also increases with increasing pentacene layer number (Figure 4c). It is expected that many-body interactions in low-dimensional materials, such as monolayer TMDs, are sensitive to dielectric environment.[30] Larger dielectric screening effect can lead to smaller trion binding energy and lower PL intensity ratio between trion and exciton.[30,43] The dielectric constant of pentacene, h-BN, and $SiO_2$ has the following ranking: h-BN > $SiO_2$ > pentacene.[43,44] Therefore, the pentacene layer with lower dielectric constant will reduce the total screening effect on the 1L $MoSe_2$ sitting on top, leading to the enhanced trion binding energy of $MoSe_2$ in the heterostructures compared with that in the 1L $MoSe_2$ sample on $SiO_2$/Si (Figure 4d–f). In addition, the thicker pentacene layer can lead to the more reduced dielectric screening, thus higher trion binding energy (Figure 4b) and higher ratio of PL intensity between trions and excitons (Figure 4c). The photoexcitation induced charge transfer within the heterostructures, from the small excitation power used, has a negligible effect on the ratio of PL intensity between trions and excitons (Note S6, Supporting Information). Our results provide a general way to precisely engineer the many-body interactions in atomically thin semiconductors, triggering new applications in ultrathin spintronic and valleytronic devices.

In conclusion, we have demonstrated an O–I 2D vdW heterojunction comprising of ultrathin organic pentacene and monolayer $MoSe_2$. Our PL and PLE measurements strongly suggest the type-I band alignments in those heterostructures, which provide a powerful platform to explore the efficient and layer-dependent exciton pumping across the O–I interfaces. The interfacial exciton pumping efficiency could be up to ≈86 times higher than the photoexcitation pumping in 1L $MoSe_2$, considering that the pentacene layer has much lower optical absorption. The high interfacial exciton pumping efficiency is related to ultrafast energy transfer across the O–I interfaces, the high quantum yields of the organic semiconductors, and the relaxation pathways of the photoexcited carriers in the hybrid system. The layer-dependent pumping efficiency is also highly related to the layer-dependent carrier transport in the atomically thin pentacene layers. Moreover, the hybridization of those atomically thin organic 2D materials has significantly modulated the many-body interactions in the monolayer $MoSe_2$ via precise dielectric engineering. Our demonstrations provide a general and new way to manipulate the exciton pumping and to engineer the many-body interactions in atomically thin semiconductors, enabling various novel and exciting optoelectronic implications in lighting, energy harvesting, spintronic and valleytronic devices, etc.

## Experimental Section

*Device Fabrication and Characterization*: Ultrathin 2D pentacene single-crystal samples were fabricated through the physical vapor deposition method over few-layer h-BN films on a $SiO_2$/Si substrate (290 nm thermal oxide on $p^+$-doped silicon).[14] The pentacene films were characterized by optical microscopy, AFM, and Raman spectroscopy to identify the number of layers and topological information. Pentacene-layer-dependent heterostructures were fabricated by dry transfer of 1L $MoSe_2$ flakes on the designated pentacene samples. For the MOS structure, used for back gate-dependent PL measurements, the 100 nm thick gold electrode was transferred to contact part of the $MoSe_2$ flakes as the probing pad.

*Optical Characterization*: PL and Raman measurements were conducted using a Horiba LabRAM system equipped with a confocal microscope, a charge-coupled device (CCD) Si detector, and a 532 nm diode-pumped solid-state (DPSS) laser as the excitation source. For temperature-dependent (above 83 K) measurements, the sample was placed into a microscope-compatible chamber with a low-temperature controller (using liquid nitrogen as the coolant). The electrical bias was applied using a Keithley 4200 semiconductor analyzer. The μ-PLE system employed in this study was a Horiba LabRAM system equipped with confocal optics and a CCD array silicon detector. A supercontinuum excitation light source (NKT SuperK Extreme EXR-20) with a tunable wavelength range between 490 and 2000 nm was employed. In this work, excitation wavelengths between 490 and 750 nm were used with a bandwidth of 12 nm for the chosen wavelengths, and the on-sample power was kept constant for all excitation wavelengths. The wavelength selection was achieved using a SuperK VARIA attachment allowing the tuning of both the center wavelength and the bandwidth of the filtered light. The laser light was focused on the sample surface via an objective lens. The diameter of the illuminated spot on the samples is ≈2 μm. The spectral response of the entire system was determined with a calibrated halogen-tungsten light source. Time-resolved PL (TRPL) measurements were conducted in a setup that incorporates micro-PL spectroscopy with a time-correlated single-photon counting (TCSPC) system. A linearly polarized pulsed laser (frequency doubled to 522 nm, with a 300 fs pulse width and a 20.8 MHz repetition rate) was directed to a high numerical aperture (NA = 0.7) objective (Nikon S Plan 60×). The PL signal was collected by a grating spectrometer, thereby either recording the PL spectrum through the CCD (Princeton Instruments, PIXIS) or detecting the PL intensity decay by a Si single-photon avalanche diode and the TCSPC (PicoHarp 300) system with a resolution of 20 ps. All the PL spectra were corrected for the instrument response. All the optical path length (OPL) characterizations were obtained using a phase-shifting interferometer (Vecco NT9100).

## Supporting Information

Supporting Information is available from the Wiley Online Library or from the author.

## Acknowledgements

L.L.Z. and A.S. contributed equally to this work. The authors would like to acknowledge the facility support from Prof. Chennupati Jagadish's group at the ANU, ACT node of the Australian National Fabrication Facility (ANFF). The authors also acknowledge financial support from ANU Ph.D. student scholarship, China Scholarship Council, ANU Major Equipment Committee fund (No. 14MEC34), and Australian Research Council (ARC) Discovery Early Career Researcher Award (DECRA) (DE140100805). ARC Centre of Excellence in Future Low-Energy Electronics Technologies (FLEET), ANU node; this work is also supported by NSFC 61734003, 61521001 and National Key Basic Research Program of China 2015CB921600. Y.R.L. and X.R.W. conceived and supervised the project; L.L.Z., Y.H.Z., Y.J.C., B.L., X.S., and A.K. prepared the samples; H.N. and D.M. contributed to the PLE setup; L.L.Z. and B.W.W. conducted the measurements; L.L.Z. did the PSI measurements. L.L.Z., A.S., and Y.Z. did the PL measurements; B.W.W., M.H.D., B.W., H.N., D.M., Z.Y.L., and Y.S. contributed to data analysis; Z.W. and Z.F.Y. did the absorption simulation; Y.R.L., L.L.Z., and A.S. cowrote the paper; all authors discussed the results and commented on the manuscript.

## Conflict of Interest

The authors declare no conflict of interest.

## Keywords

2D materials, binding energy, exciton pumping, organic–inorganic, type-I heterostructures

Received: June 23, 2018
Revised: July 19, 2018
Published online:

[1] G.-H. Lee, C.-H. Lee, A. M. van der Zande, M. Han, X. Cui, G. Arefe, C. Nuckolls, T. F. Heinz, J. Hone, P. Kim, *APL Mater.* **2014**, *2*, 092511.
[2] Y. C. Lin, R. K. Ghosh, R. Addou, N. Lu, S. M. Eichfeld, H. Zhu, M. Y. Li, X. Peng, M. J. Kim, L. J. Li, R. M. Wallace, S. Datta, J. A. Robinson, *Nat. Commun.* **2015**, *6*, 7311.
[3] C.-H. Lee, G.-H. Lee, A. M. van der Zande, W. Chen, Y. Li, M. Han, X. Cui, G. Arefe, C. Nuckolls, T. F. Heinz, J. Guo, J. Hone, P. Kim, *Nat. Nanotechnol.* **2014**, *9*, 676.
[4] Q. H. Wang, K. Kalantar-Zadeh, A. Kis, J. N. Coleman, M. S. Strano, *Nat. Nanotechnol.* **2012**, *7*, 699.
[5] D. Jariwala, S. L. Howell, K. S. Chen, J. Kang, V. K. Sangwan, S. A. Filippone, R. Turrisi, T. J. Marks, L. J. Lauhon, M. C. Hersam, *Nano Lett.* **2016**, *16*, 497.
[6] S. B. Homan, V. K. Sangwan, I. Balla, H. Bergeron, E. A. Weiss, M. C. Hersam, *Nano Lett.* **2016**, *17*, 164.
[7] E. H. Cho, W. G. Song, C. J. Park, J. Kim, S. Kim, J. Joo, *Nano Res.* **2014**, *8*, 790.
[8] D. Jariwala, T. J. Marks, M. C. Hersam, *Nat. Mater.* **2017**, *16*, 170.
[9] T. Zhu, L. Yuan, Y. Zhao, M. W. Zhou, Y. Wan, J. G. Mei, L. B. Huang, *Sci. Adv.* **2018**, *4*, 8.
[10] X. Liu, J. Gu, K. Ding, D. Fan, X. Hu, Y. W. Tseng, Y. H. Lee, V. Menon, S. R. Forrest, *Nano Lett.* **2017**, *17*, 3176.
[11] F. Zhang, Y. Ma, Y. Chi, H. Yu, Y. Li, T. Jiang, X. Wei, J. Shi, *Sci. Rep.* **2018**, *8*, 8208.
[12] H. Ozaki, *J. Chem. Phys.* **2000**, *113*, 6361.
[13] C. Menozzi, V. Corradini, M. Cavallini, F. Biscarini, M. G. Betti, C. Mariani, *Thin Solid Films* **2003**, *428*, 227.
[14] Y. Zhang, J. Qiao, S. Gao, F. Hu, D. He, B. Wu, Z. Yang, B. Xu, Y. Li, Y. Shi, W. Ji, P. Wang, X. Wang, M. Xiao, H. Xu, J. B. Xu, X. Wang, *Phys. Rev. Lett.* **2016**, *116*, 016602.
[15] D. He, Y. Zhang, Q. Wu, R. Xu, H. Nan, J. Liu, J. Yao, Z. Wang, S. Yuan, Y. Li, Y. Shi, J. Wang, Z. Ni, L. He, F. Miao, F. Song, H. Xu, K. Watanabe, T. Taniguchi, J. B. Xu, X. Wang, *Nat. Commun.* **2014**, *5*, 5162.
[16] I. G. Hill, A. Kahn, Z. G. Soos, R. A. Pascal, *J. Chem. Phys. Lett.* **2000**, *327*, 8.
[17] S. Nakamura, M. Senoh, N. Iwasa, S.-I. Nagahama, *Jpn. J. Appl. Phys.* **1995**, *34*, 3.
[18] C. Hui, K. Jun, S. Hasan, C. Bin, S. Aslihan, W. Kedi, P. Francois, M. Xiuqing, T. Sefaattin, *Nanotechnology* **2016**, *27*, 065203.
[19] M. Z. Bellus, M. Li, S. D. Lane, F. Ceballos, Q. Cui, X. C. Zeng, H. Zhao, *Nanoscale Horiz.* **2017**, *2*, 31.
[20] S. J. Kang, G.-H. Lee, Y.-J. Yu, Y. Zhao, B. Kim, K. Watanabe, T. Taniguchi, J. Hone, P. Kim, C. Nuckolls, *Adv. Funct. Mater.* **2014**, *24*, 5157.
[21] G. H. Lee, Y. J. Yu, X. Cui, N. Petrone, C. H. Lee, M. S. Choi, D. Y. Lee, C. G. Lee, W. J. Yoo, K. J. Watanabe, T. Taniguchi, C. Nuckolls, P. Kim, J. Hone, *ACS Nano* **2013**, *7*, 6.
[22] M. Florian, M. Hartmann, A. Steinhoff, J. Klein, A. W. Holleitner, J. J. Finley, T. O. Wehling, M. Kaniber, C. Gies, *Nano Lett.* **2018**, *18*, 2725.
[23] A. Castellanos-Gomez, M. Buscema, R. Molenaar, V. Singh, L. Janssen, H. S. J. van der Zant, G. A. Steele, *2D Mater.* **2014**, *1*, 011002.
[24] Y. Gong, J. Lin, X. Wang, G. Shi, S. Lei, Z. Lin, X. Zou, G. Ye, R. Vajtai, B. I. Yakobson, H. Terrones, M. Terrones, B. K. Tay, J. Lou, S. T. Pantelides, Z. Liu, W. Zhou, P. M. Ajayan, *Nat. Mater.* **2014**, *13*, 1135.
[25] X. Hong, J. Kim, S. F. Shi, Y. Zhang, C. Jin, Y. Sun, S. Tongay, J. Wu, Y. Zhang, F. Wang, *Nat. Nanotechnol.* **2014**, *9*, 682.
[26] V. O. Özcelik, J. G. Azadani, C. Yang, S. J. Koester, T. Low, *Phys. Rev. B* **2016**, *94*, 035125.
[27] C. Gong, H. Zhang, W. Wang, L. Colombo, R. M. Wallace, K. Cho, *Appl. Phys. Lett.* **2013**, *103*, 053513.
[28] H. Yoshida, K. Yamada, J. Y. Tsutsumi, N. Sato, *Phys. Rev. B* **2015**, *92*, 075145.
[29] M. Shionoiri, M. Kozasa, S. Kera, K. K. Okudaira, N. Ueno, *Jpn. J. Appl. Phys.* **2007**, *46*, 1625.
[30] J. Pei, J. Yang, X. Wang, F. Wang, S. Mokkapati, T. Lu, J. C. Zheng, Q. Qin, D. Neshev, H. H. Tan, C. Jagadish, Y. Lu, *ACS Nano* **2017**, *11*, 7468.
[31] P. Tonndorf, R. Schmidt, P. Böttger, X. Zhang, J. Börner, A. Liebig, M. Albrecht, C. Kloc, O. Gordan, D. R. T. Zahn, S. M. Vasconcellos, R. Bratschitsch, *Opt. Express* **2013**, *21*, 9.
[32] J. S. Ross, S. Wu, H. Yu, N. J. Ghimire, A. M. Jones, G. Aivazian, J. Yan, D. G. Mandrus, D. Xiao, W. Yao, X. Xu, *Nat. Commun.* **2013**, *4*, 1474.
[33] A. Rao, M. W. B. Wilson, S. Albert-Seifried, R. Di Pietro, R. H. Friend, *Phys. Rev. B* **2011**, *84*, 195411.
[34] M. Amani, D. H. Lien, D. Kiriya, J. Xiao, A. Azcatl, J. Noh, S. R. Madhvapathy, R. Addou, S. KC, M. Dubey, K. Cho, R. M. Wallace, S. Lee, J. He, J. W. Ager III, X. Zhang, E. Y. A. Javey, *Science* **2015**, *350*, 4.
[35] M. Palummo, M. Bernardi, J. C. Grossman, *Nano Lett.* **2015**, *15*, 2794.
[36] D. Kozawa, R. Kumar, A. Carvalho, A. K. Kumar, W. Zhao, S. Wang, M. Toh, R. M. Ribeiro, A. H. C. Neto, K. Matsuda, G. Eda, *Nat. Commun.* **2014**, *5*, 4543.
[37] M. Tabachnyk, B. Ehrler, S. Gelinas, M. L. Bohm, B. J. Walker, K. P. Musselman, N. C. Greenham, R. H. Friend, A. Rao, *Nat. Mater.* **2014**, *13*, 1033.
[38] A. Rao, M. W. B. Wilson, M. H. Justin, A.-S. Sebastian, B. Heinz, R. H. Friend, *J. Am. Chem. Soc.* **2010**, *132*, 6.
[39] A. Sharma, H. Yan, L. Zhang, X. Sun, B. Liu, Y. Lu, *Acc. Chem. Res.* **2018**, *51*, 1164.
[40] M. M. Ugeda, A. J. Bradley, S. F. Shi, F. H. da Jornada, Y. Zhang, D. Y. Qiu, W. Ruan, S. K. Mo, Z. Hussain, Z. X. Shen, F. Wang, S. G. Louie, M. F. Crommie, *Nat. Mater.* **2014**, *13*, 1091.
[41] J. Yang, T. Lu, Y. W. Myint, J. Pei, D. Macdonald, J.-C. Zheng, Y. Lu, *ACS Nano* **2015**, *9*, 7.
[42] I. Kylänpää, H.-P. Komsa, *Phys. Rev. B* **2015**, *92*, 205418.
[43] Y. Lin, X. Ling, L. Yu, S. Huang, A. L. Hsu, Y. H. Lee, J. Kong, M. S. Dresselhaus, T. Palacios, *Nano Lett.* **2014**, *14*, 5569.
[44] C. H. Kim, O. Yaghmazadeh, D. Tondelier, Y. B. Jeong, Y. Bonnassieux, G. Horowitz, *J. Appl. Phys.* **2011**, *109*, 083710.